Pericyclic versus Pseudopericyclic Reactions. What the Laplacian of the Charge Density, $\nabla^2\rho(r)$, Has To Say about It? The Case of Cycloaddition Reactions

Saturnino Calvo-Losada and J. J. Quirante Sánchez*

Departamento de Química Física, Facultad de Ciencias, Campus de Teatinos, s/n, Universidad de Málaga, 29071 Málaga, Spain

Received: December 7, 2007; Revised Manuscript Received: April 25, 2008

The pseudopericyclic character of a group of cycloaddition reactions is theoretically investigated with the quantum theory of atoms in molecules of Bader at B3LYP/6-311++G(d,p) and MP2/6-311++G(d,p) levels of theory. The analysis of the topology of the Laplacian of the charge density, $\nabla^2\rho(r)$, along the reaction coordinate sets out a clear cut between pericyclic and pseudopericyclic processes and also allows one to account for intermediate cases.

Introduction

In 1976, Lemal and co-workers proposed the name pseudopericyclic to describe an extraordinarily facile sigmatropic pathway for automerization of a sulfoxide group.[1] Lemal said, "A pseudopericyclic reaction is a concerted transformation whose primary changes in bonding compass a cyclic array of atoms, at one (or more) of which nonbonding and bonding atomic orbitals interchange roles". In the crucial sense the role interchange means a "disconnection" in the cyclic array of overlapping orbitals because the atomic orbitals switching functions are mutually orthogonal." Hence, pseudopericyclic reactions cannot be orbital symmetry forbidden.

Nearly 20 years later, Birney,[2–10] after dealing with a great number of possible pseudopericyclic mechanisms, arrived at the following conclusions: the pseudopericyclic transition structure (TS) (a) is almost planar (when possible),[7] (b) exhibits no significant barrier of energy, and (c) is ever symmetry allowed. Yet, some problems remain unsolved, such as no definitive criterion which allows a pseudopericyclic reaction to be distinguished from a normal pericyclic reaction.[11] There is also a certain controversy regarding how many disconnections define a pseudoperyciclic TS and their proper origin. Different theoretical approaches have been used to deal with disconnections: Rodríguez Otero, Cabaleiro-Lago, et al.[11–17] have made use of the ACID method developed by Herges.[18–20] For its part, de Lera et al. have recently proposed a criterion based on the ellipticity.[21] Rode and Dobrowolski have associated disconnections with absent bond critical points in the electronic charge density $\rho(\boldsymbol{r})$.[22,23] Chamorro et al.[24–28] and Matito et al.[28,29] have applied ELF methodology[30] to determine the nature of bonding in several pseudopericyclic reactions. Alajarín et al. have reported several reactions where two pseudopericyclic processes did occur consecutively.[31]

In this paper, we present preliminary results of a series of studies considering some cycloaddition reactions previously considered by Cabaleiro-Lago et al.[11] (see Scheme 1) by using the Laplacian of the charge density, $\nabla^2\rho(\boldsymbol{r})$, in the framework of the quantum theory of atoms in molecules (QTAIM) developed by Bader.[32] A detailed analysis of the topology of $\nabla^2\rho(\boldsymbol{r})$ along the reaction coordinate will provide clear mechanistic differences between pericyclic and pseudopericyclic processes. We will also check the criterion for electrocyclizations proposed by de Lera et al. on the basis of the ellipticity of the charge density and its suitability for cycloadditions.[13] As we will see, there is no need to invoke disconnections in the orbital array at the TS because the QTAIM makes use of the electronic density instead of the molecular orbitals.

SCHEME 1: Cycloaddition Reactions Considered in this Study

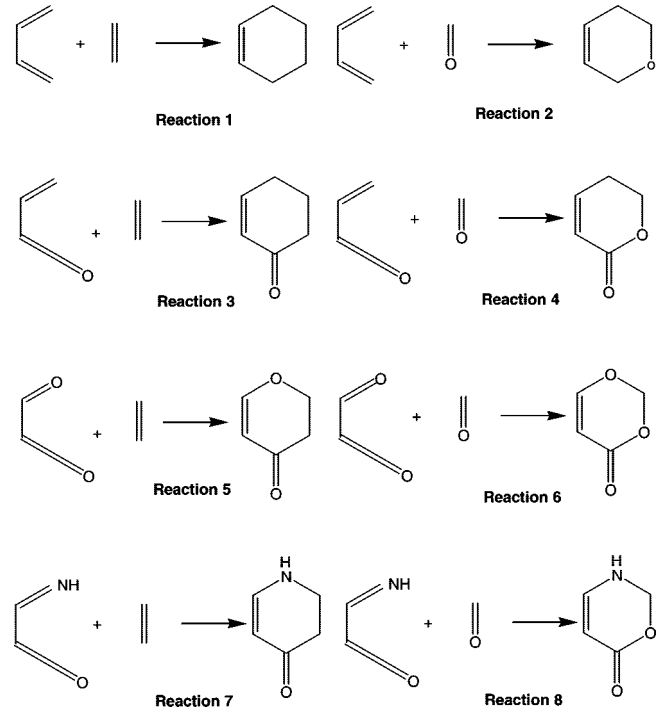

Theoretical Methods

In the QTAIM developed by R. F. W. Bader,[32] the topology of the charge density distribution, $\rho(\boldsymbol{r})$, and the laplacian, $\nabla^2\rho(\boldsymbol{r})$, are analyzed through their critical points (CPs). The topological analysis of $\rho(\boldsymbol{r})$ renders CPs that can be associated with every molecular element: maxima (3, −3) with nuclei, saddle (3, −1) and (3, +1) points with bonds (BCPs) and rings (RCPs), respectively, and minima (3, +3) with cages. Where the CPs

* Corresponding author. E-mail: quirante@uma.es.

10.1021/jp711565g CCC: $40.75
Published on Web 08/13/2008

SCHEME 2: Atomic Graph for a Trigonal and Tetrahedral Carbon Atom

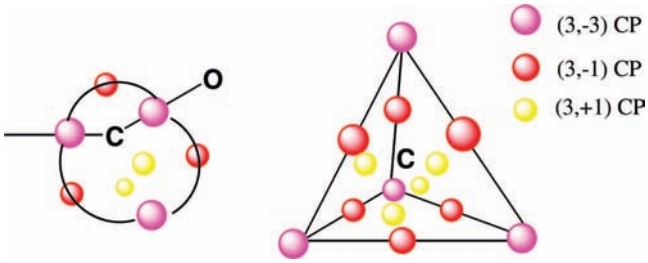

TABLE 1: Energy Barriers computed at B3LYP and MP2 with (1) 6-31G(d) and (2) 6-311++G(d,p) basis sets (ZPVE included) for the TSs with respect to the minima obtained from the IRC calculations

	B3LYP/1[a]	B3LYP/2[a]	MP2/1[b]	MP2/2[b]
TS1	21.75	24.11	19.14	21.11
TS2	22.77	24.51	24.09	23.17
TS3	22.54	25.18	20.08	
TS4	14.59	17.16	17.37	16.83
TS5	21.74	25.12	28.13	28.89
TS6	5.70	8.09	11.57	13.28
TS7	22.82	25.53	24.38	23.95
TS8	5.26	7.02	10.24	11.20

[a] ZPVE computed at B3LYP/6-31G(d) is included. [b] ZVPE computed at MP2/6-31G(d) is included.

are characterized by the signature and the rank, that is, the number of non-zero eigenvalues and the algebraic sum of their signs, respectively. The Poincaré−Hopf condition (nuclei − bonds + rings − cages = 1) is usually fulfilled.

In this theory, the Laplacian of the charge density is of crucial importance to recover the reactivity sites.[33–41] This scalar field appears in the QTAIM in the local form of the virial theorem $2G(\boldsymbol{r}) + V(\boldsymbol{r}) = (h^2/8\pi m)\nabla^2\rho(\boldsymbol{r})$, being connected with the Hellmann−Feynmann and Ehrenfest forces[32] and providing ultimately the mechanics of the atom within the molecule.

Furthermore, because it expresses the local balance between the potential and kinetic contributions to $\rho(\boldsymbol{r})$, the scalar field allows one to characterize the atomic interactions[32,42,43] by means of properties computed at the BCP: $\rho(\boldsymbol{r}_c)$, $\nabla^2\rho(\boldsymbol{r}_c)$ ($= \lambda_1 + \lambda_2 + \lambda_3$, i.e.. the trace of the Hessian matrix evaluated at the corresponding BCP), λ_1, λ_2, and λ_3 (the former correspond to eigenvectors perpendicular to the bond and the latter to that parallel), the ellipticity ($\varepsilon = \lambda_1/\lambda_2 - 1$, which gives information about the distribution of $\rho(\boldsymbol{r})$ around the interaction line), the local energy density $H(\boldsymbol{r}) = -K(\boldsymbol{r})$, proposed by Cremer and Kraka,[44] kinetic energy densities $G(\boldsymbol{r})$ and $K(\boldsymbol{r})$ evaluated at the bond CP, and the ratio $G(\mathbf{r})/\rho(\boldsymbol{r})$.[32,42] Other derivative magnitudes have been tested by Gibbs et al.[45]

When $V(\mathbf{r})$ dominates upon $G(\mathbf{r})$, $\nabla^2\rho(\boldsymbol{r}) < 0$, and the charge density is accumulated in the BCP, resulting eventually in a shared interaction. On the other hand, when $G(\mathbf{r})$ dominates upon $V(\mathbf{r})$, $\nabla^2\rho(\boldsymbol{r})$ becomes positive, and the charge density is displaced towards the basins of the nuclei, therefore exhibiting low values of $\rho(\boldsymbol{r})$ and nearly zero values of $\nabla^2\rho(\boldsymbol{r})$ at the BCP. These are closed-shell interactions that appear in ionic, van der Waals complexes, and so forth. Intermediate interactions (or polar shared interaction) are found out in heteronuclear bonds with great values of $\rho(\boldsymbol{r}_c)$, but $\nabla^2\rho(\boldsymbol{r}_c) > 0$ because of the effect of polarization of the charge density towards the basin of the more electronegative atom ($\lambda_3 > \lambda_1 + \lambda_2$).[32]

Similarly to $\rho(\boldsymbol{r})$, the topological analysis of the laplacian of the charge density renders CPs associated with local charge accumulation ($\nabla^2\rho(\boldsymbol{r}) < 0$) and depletion ($\nabla^2\rho(\boldsymbol{r}) > 0$). Local maxima (3, −3) and minima (3, +3) in $L(\boldsymbol{r}) = -\nabla^2\rho(\boldsymbol{r})$ will indicate sites with local accumulation and local depletion of charge, respectively. There are also (3, +1) and (3, −1) saddle points. As Popelier points out, the topology of $\nabla^2\rho(\boldsymbol{r})$ is extremely complex, and up to now, only full topologies for simple molecules (H_2O and NH_3) have been reported.[38,39]

The $\nabla^2\rho(\boldsymbol{r})$ accounts for the shell structure of the atom: a charge concentration (CC) shell is accompanied with a charge depletion (CD) one.[38,39] The more external shell of CC is the valence shell of CC (VSCC) and is of primary interest for dealing with chemical reactivity. Upon combination, (3, −3) CPs associated with bonded (BP) and nonbonded CCs (3, −3)LP (so denoted because they are usually located where a electronic lone pair is expected), saddle points (3, −1), and local minima (3, +1), the so-called holes, are exhibited. These points form the atomic graph of an atom with the (3, −3) CPs at the vertices, the (3, −1)CPs at the edges, and the (3, +1) CPs at the center of each face (see Scheme 2) and also fulfill the Poincaré−Hopf rule (vertices − edges + faces = 2). Facing the (3, +1) CPs in VSCC, one can also find (3, +3)CPs in the VSCD as in donor−acceptor complexes.[38–40]

$\nabla^2\rho(\boldsymbol{r})$ recovers Lewis acid−base reactions in a general sense through the alignment of a Lewis base or nucleophile (caracterized by a (3, −3) CP or a lump) with a Lewis acid or electrophile (characterized by a (3, +1) or a hole).[32,38–40] Moreover, it allows one to extend the concept of Lewis acid and base by considering secondary local accumulations, (3, −1) CPs.[33,40] These CPs are saddle points within the VSCC but local maxima with respect to points outside the VSCC. In a bonding stable situation, each atom contributes to the bond with a (3, −3) CP in the VSCC, being also a (3, −1) CP associated with the BCP of $\rho(\boldsymbol{r})$.[32] In some bonding situations (as in ethers), the oxygen atom provides a (3, −1) CP in its VSCC that is actually a (3, −3) CP in the direction of the interaction line. A recent review by Cortes-Guzmán and Bader[40] has also shown that $L(\mathbf{r}) = -\nabla^2\rho(\boldsymbol{r})$ can recover the ligand field theory where the ligands are linked to the metal through (3, −3) CCs in the donor with holes in the acceptor (via (3, +3) or (3, +1) CPs, alternatively)[40] but remarkably without a (3, −1) CP in between. In van der Waals complexes, a lump−hole alignment has also been detected.[41]

Computations

All the geometries were computing with GAUSSIAN98[46] and GAUSSIAN 2003[47] software. The topology of the scalar fields $\rho(\boldsymbol{r})$ and $\nabla^2\rho(\boldsymbol{r})$ were analyzed with the AIM2000 v.1 software[48] and MORPHY98 automated program.[49] Optimizations were performed at B3LYP[50] and MP2 with 6-31G(d) and 6-311++G(d,p) basis sets,[51] and the charge density was built up from the wave function at the same level of theory. The TSs were confirmed by frequency calculations at B3LYP/6-31G(d) and MP2/6-31G(d) levels of theory. The normal modes of vibration were visualized with MOLDEN.[52] From the TS obtained for each process, subsequent IRC[53] calculations were performed at B3LYP/6-311++G(d,p) (computing the analytic Hessian at the first point) and yielded minima that were subsequently reoptimized at both B3LYP and MP2 levels of theory with the same basis set. In some cases (as in **TS7**), it was necessary to compute the analytic Hessian at every point to achieve convergence at B3LYP/6-311++G(d,p). Nevertheless, the criteria of conver-

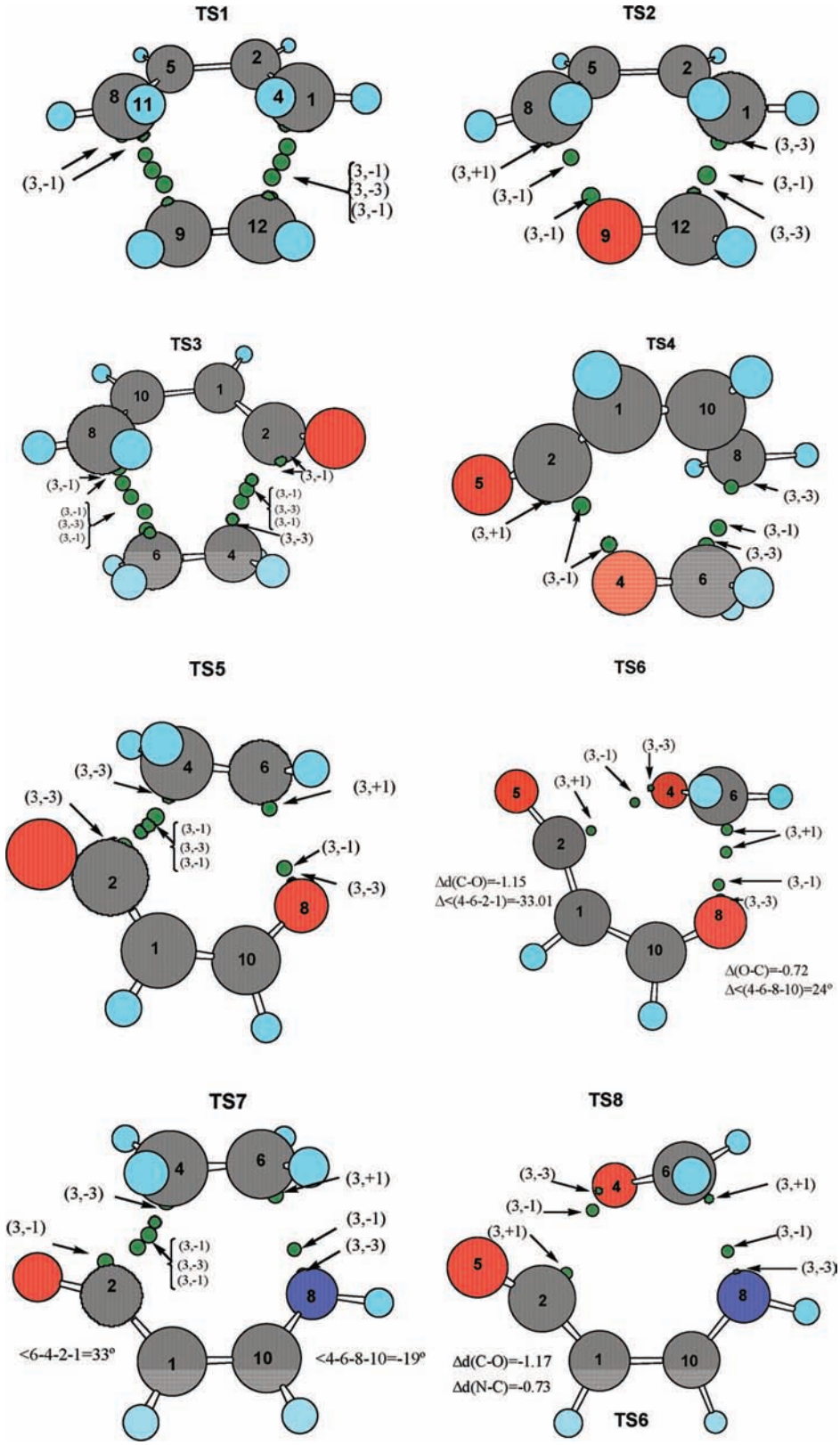

Figure 1. Geometries of TS structures and CPs of $L(\boldsymbol{r})$ involved in bond formation computed at B3LYP/6-311++G(d,p).

gence of GAUSSIAN where not completely achieved for **TS3** at MP2/6-311++G(d,p) (Maximum Force: 0.042114 instead of 0.00450 and RMS 0.006045 instead of 0.000300). From the intermediate IRC geometries, the laplacian $\nabla^2\rho(\boldsymbol{r})$ was built up at MP2/-6-311++G(d,p), and analysis of the CPs along the reaction coordinate was subsequently performed.

Results

Energetics and Geometries. The energy barriers (with the ZPVE included) computed at B3LYP and MP2 with (1) 6-31G(d) and (2) 6-311++G(d,p) basis sets for the TSs considered in this study with respect to the minima are collected in Table 1.

Reactant	TS	Product

Reaction 1

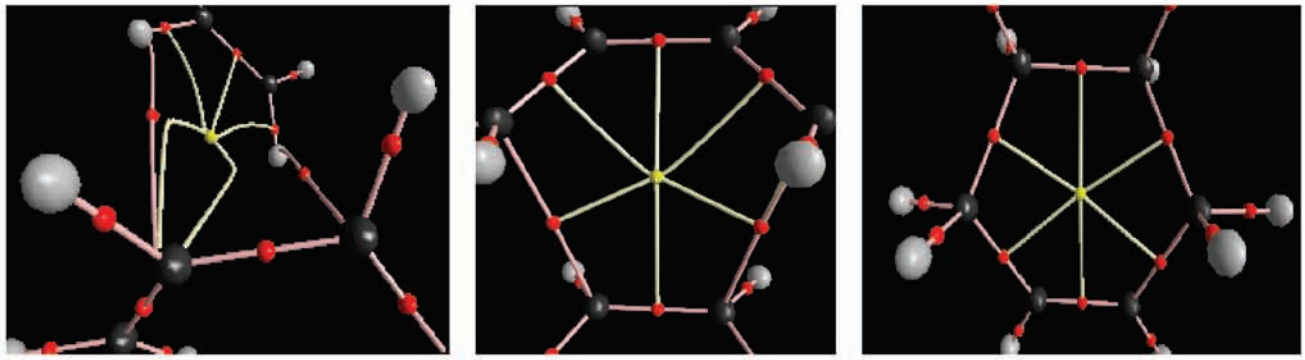

Reaction 2

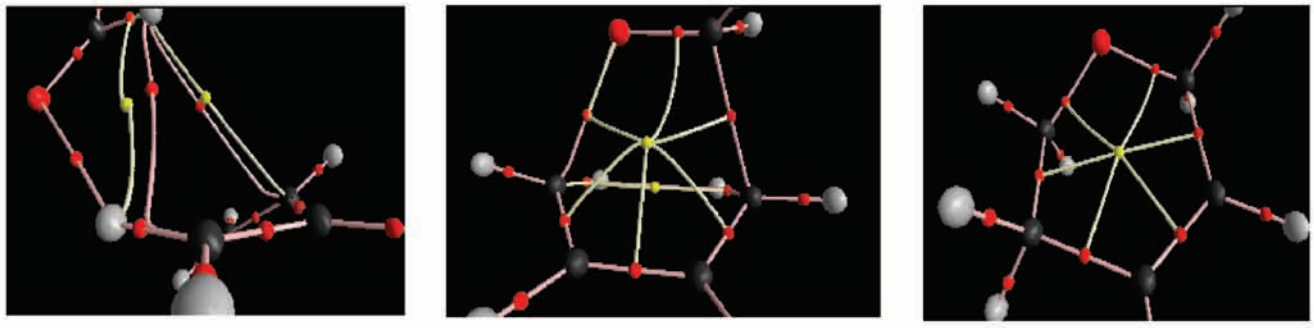

Reaction 3

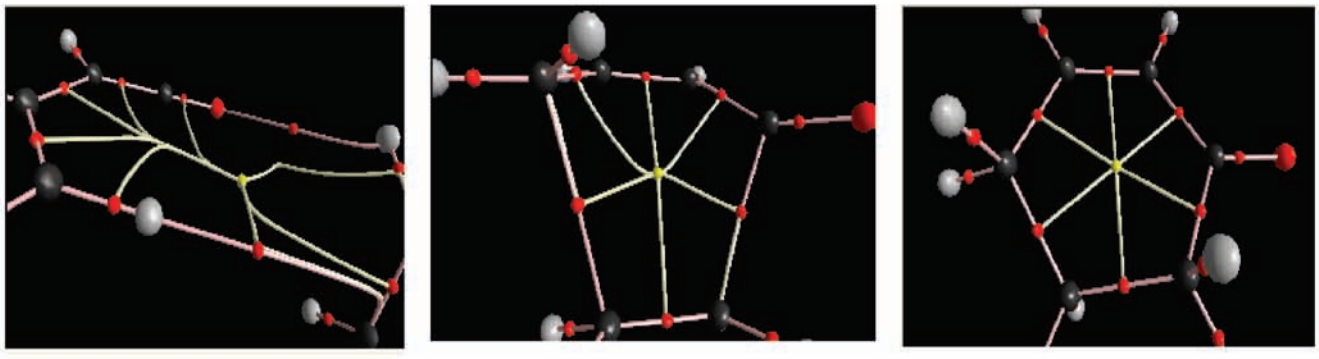

Reaction 4

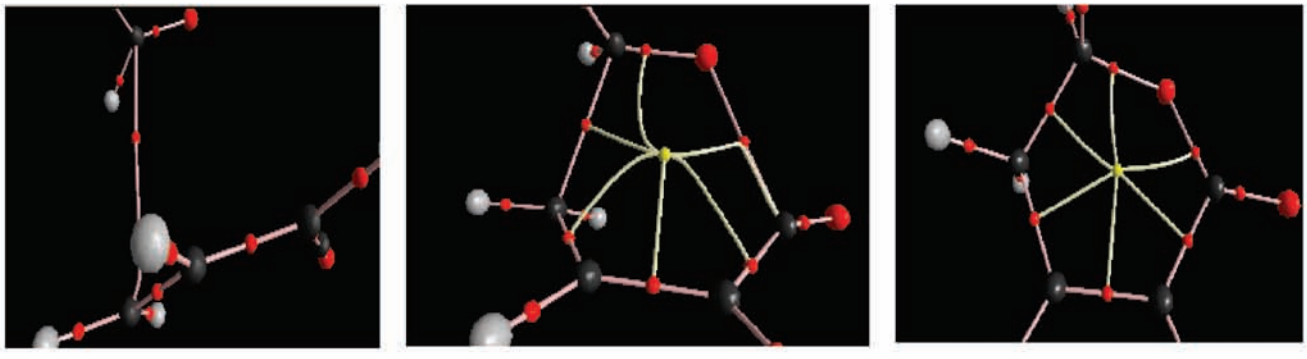

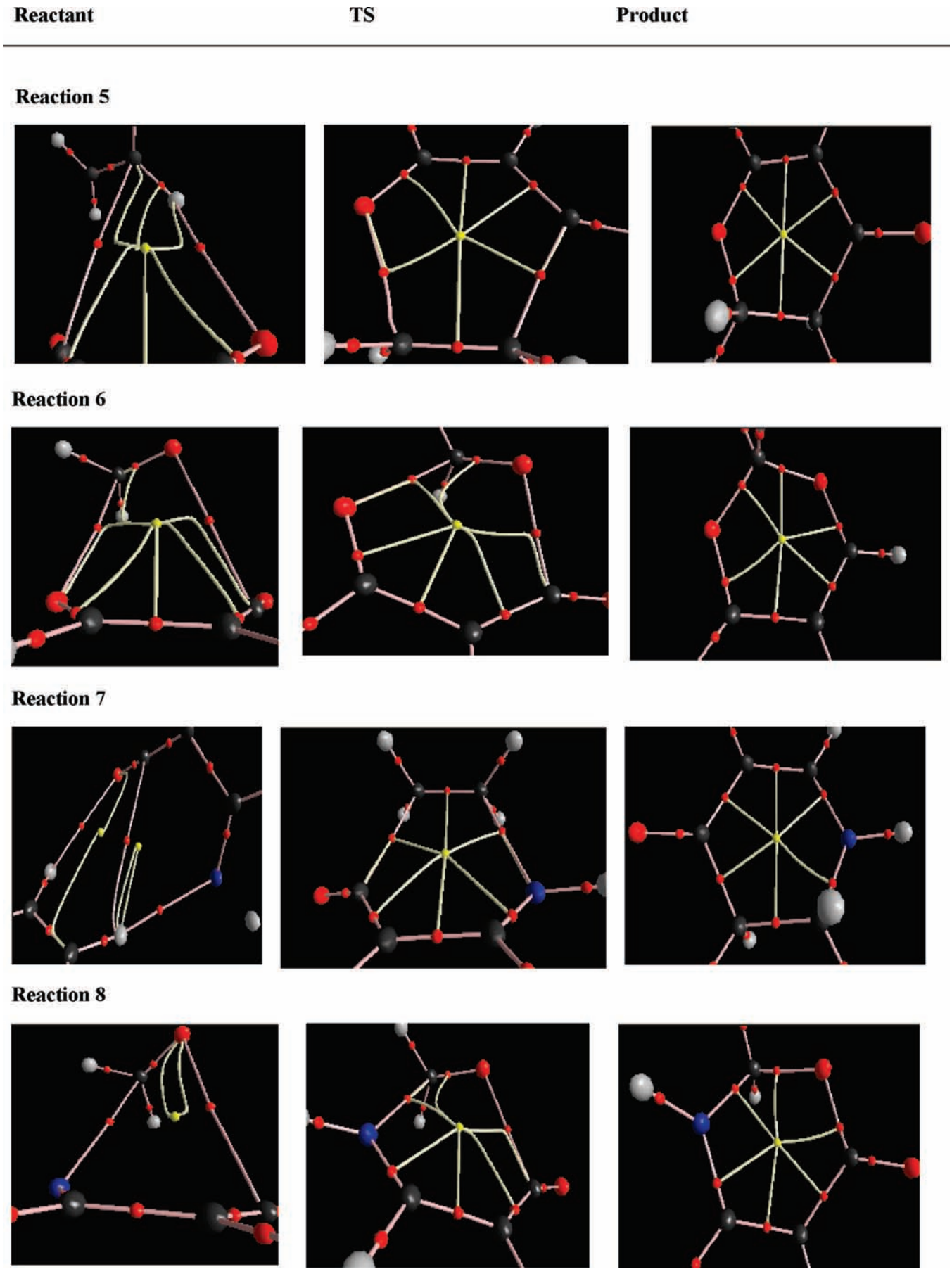

Figure 2. Molecular graphs derived from trajectories of $\nabla\rho(\mathbf{r})$ and CPs from $\rho(\mathbf{r})$ for Reactions of Scheme 1 computed from densities at MP2/6-311++(d,p)//MP2/6-311++G(d,p) for reactants and B3LYP/6-311++G(d,p)//B3LYP/6-311++G(d,p) for TSs and products (red points represent BCPs and yellow ones stand for RCPs).

TABLE 2: Relevant Properties of $\rho(r)$ Computed at BCPs for the Bonds Being Formed in the TSs at B3LYP/6-311++G(d,p) Level of Theory[a]

	$\rho(\mathbf{r}_c)$	$\nabla^2\rho(\mathbf{r}_c)$	ε	$H(\mathbf{r}_c)$	$G(\mathbf{r}_c)$	λ_1	λ_2	λ_3	$G(\mathbf{r}_c)/\rho(\mathbf{r}_c)$
				TS1					
C12−C1	0.05093	0.04380	0.14892	−0.00898	0.01993	−0.05391	−0.0692	0.14463	0.3913
C9−C8	0.05093	0.04380	0.14892	−0.00898	0.01993	−0.05391	−0.0692	0.14463	0.3913
				TS2					
C12−C1	0.08593	0.00999	0.12519	−0.02819	0.03068	−0.11214	−0.09966	0.22180	0.3570
C8−O9	0.05440	0.12657	0.31725	−0.00326	0.03490	−0.06747	−0.05122	0.24527	0.6415
				TS3					
C2−C4	0.06052	0.03695	0.09966	−0.01320	0.02244	−0.07171	−0.06521	0.17387	0.3708
C6−O8	0.04528	0.04839	0.16066	−0.00680	0.01890	−0.04496	−0.03874	0.13209	0.4174
				TS4					
C6−C8	0.07639	0.02503	0.14236	−0.02261	0.02886	−0.09527	−0.08340	0.20369	0.3778
C2−O4	0.05143	0.12919	0.23655	−0.00234	0.03464	−0.06506	−0.05262	0.24687	0.6735
				TS5					
C2−C4	0.06749	0.03269	0.01765	−0.01726	0.02543	−0.07931	−0.07793	0.18993	0.3768
C6−O8	0.04534	0.12751	0.19509	−0.00129	0.03316	−0.04764	−0.03986	0.21500	0.7313
				TS6					
C2−O4	0.05478	0.13337	0.17701	−0.00396	0.03730	−0.06987	−0.05936	0.26260	0.6809
C6−O8	0.04925	0.13143	0.14804	−0.00273	0.03558	−0.05564	−0.04846	0.23553	0.7224
				TS7					
C2−O4	0.05842	0.03981	0.09344	−0.01241	0.02237	−0.72615	−0.06195	0.16950	0.3829
C6−N8	0.04995	0.09825	0.15017	−0.00469	0.02925	−0.05364	−0.04663	0.19852	0.5856
				TS8					
C2−O4	0.03853	0.10773	0.25988	−0.00019	0.02712	−0.04427	−0.03514	0.18714	0.7039
C6−N8	0.05448	0.10836	0.12114	−0.00672	0.03381	−0.06099	−0.05440	0.22375	0.6206

[a] $\rho(\mathbf{r}_c)$, the charge density; $\nabla^2\rho(\mathbf{r}_c)$, Laplacian; ε, ellipticity; $H(\mathbf{r}_c)$, local energy density ($= -K(\mathbf{r})$); λ_1, λ_2, and λ_3, eigenvalues of the Hessian matrix; and $K(\mathbf{r})$ and $G(\mathbf{r})$, kinetic energy densities.

As can be clearly seen for **TS6** and **TS8**, the energy barriers are predicted to be very low as compared to those of **TS1**, **TS2**, **TS3**, **TS5**, and **TS7**, with a difference of about 8 and 15 kcal/mol at MP2/6-311++G(d,p) and B3LYP/6-311++G(d,p), respectively. **TS4** is half way between both extremes. Hence, according to Birney,[2–10] the criteria of practically null barrier would only be achieved by **TS6** and **TS8**. Unexpectedly, **TS1** and **TS2** are predicted to be below **TS5** at B3LYP/6-311++G(d,p), by about 1 and 0.5 kcal/mol, respectively. Furthermore, at MP2/6-311++G(d,p), this TS is predicted to be the least stable one (see Table 1).

The geometries for the TSs (**TS*n*, *n*** = 1,..., 8) predicted at B3LYP/6-311++G(d,p) level of theory together with the relevant CPs of $L(\mathbf{r})$, built up from the wavefunction at the same level, are depicted in Figure 1. As expected, the presumably pericyclic TSs (i.e., **TS1**, **TS2, TS3, TS4**, and **TS7**) are nonplanar, although **TS7** is not far from planarity (see dihedral angles in Figure 1). The pseudopericyclic TSs are not all planar (as **TS6**). The **TS5** is predicted to be planar at B3LYP/6-311++G(d,p) but non-planar at MP2/6-311++G(d,p).

Topology of $\rho(r)$. In Figure 2, the molecular graphs of TSs, reactants and products obtained from $\nabla\rho(\mathbf{r})$, and the CPs of $\rho(\mathbf{r})$ at B3LYP/6-311++G(d,p) and MP2/6-311++G(d,p) are plotted. Remarkably, for all the TS structures considered in this paper, all the BCPs corresponding to the bonds being formed were located in $\rho(\mathbf{r})$. Therefore, the closure of each TS structure is topologically reflected in the appearance of a RCP, and consequently, the Poincaré−Hopf relationship is fulfilled. This seems to be in contradiction with the proposal by Rode and Dobrowolksi commented above.[22,23] Interestingly, the values of $\rho(\mathbf{r})$ at the BCPs ($\rho(\mathbf{r}_c)$) are practically the same for all the forming bonds, but the value of $\nabla^2\rho(\mathbf{r}_c)$ differs for the C−X bonds, for which a great positive value is obtained. Furthermore, the ellipticity, ε, for all the bonds is below 0.5 au, which seems to be at odds with the proposal of López et al.[21] According to these authors, a pseudopericyclic electrocyclization TS must have an ellipticity under 0.5 (supposedly in au), being over 4 au for pericyclic di-rotatory and around 1 for pericyclic mono-rotatory. Therefore, it would seem that the values set up for electrocyclizations cannot be extrapolated to cycloadditions.

The values and signs of the parameters ($H(\mathbf{r}_c) > 0$ and $G(\mathbf{r}_c)/\rho(\mathbf{r}_c) > 1$) indicate that all fall in the domain of shared interactions. Interestingly, there is a clear difference in the magnitude of $\nabla^2\rho(\mathbf{r})$ evaluated at the corresponding BCPs: pseudopericyclic contacts show values over 0.09 au (compare C−X, X = O, N with C−C in Table 2). Moreover, the pseudopericyclic contacts show values of the ratio $G(\mathbf{r}_c)/\rho(\mathbf{r}_c)$ over 0.5 au. The latter findings could be considered as criteria to differentiate between pericyclic and pseudopericyclic reactions, but more research is needed to establish a clear cut.

A striking finding is a H−H interaction between adjacent hydrogen atoms (numbered 4 and 11 in Figure 1) in the butadiene fragment that appears in the pericylic **TS1** and **TS2** at MP2/6-311++G(d,p) ($\rho(\mathbf{r}_c) = 0.01341$ au, $\nabla^2\rho(\mathbf{r}_c) = 0.05804$ au) and at B3LYP/6-311++G(d,p) levels of theory. This kind of interaction, different from a dihydrogen bond, has also been encountered in some crystals.[54]

In order to set out more differences between both types of processes and to take into account dubious intermediate cases, the topology of $\rho(\mathbf{r})$ for the reactants were also analysed. From the TSs, IRC calculations went down to minima on the PES that upon subsequent optimization rendered diverse situations. For **TS6**, **TS8**, and **TS4**, the IRC calculations (plus subsequent optimization) rendered geometries for the reactants very similar to those of the corresponding TS (for instance, between 0.7 and 1.2 Å of difference for **TS6** and **TS8,** see Figure 1), hence the low energy barriers found. In fact, each TS is homeomorphic with respect to its respective reactant because they exhibit the

(a) TS6

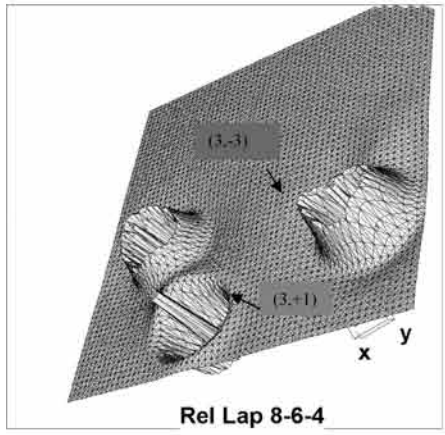

Rel Lap 8-6-4

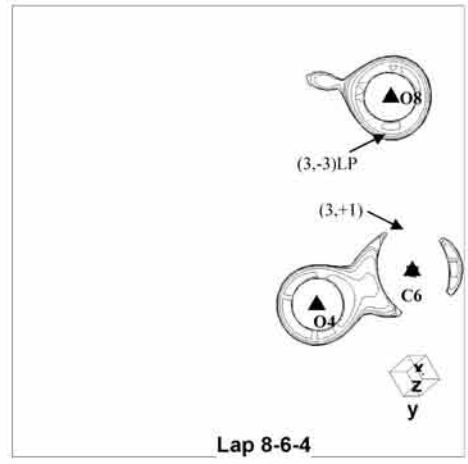

Lap 8-6-4

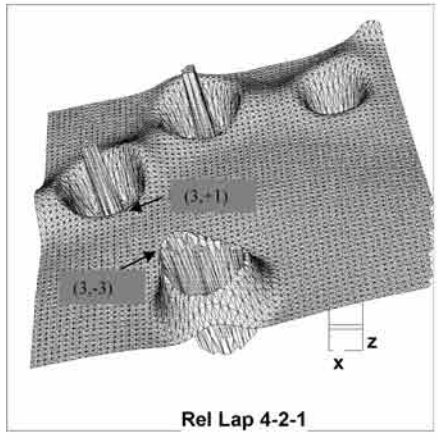

Rel Lap 4-2-1

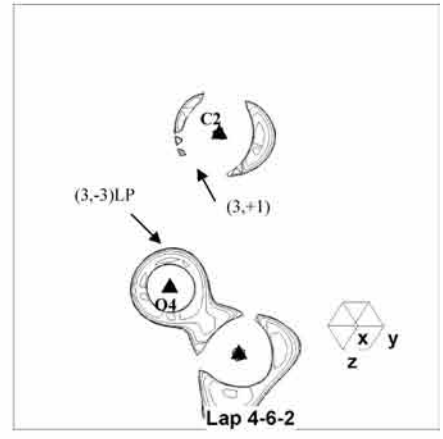

Lap 4-6-2

(b) TS1

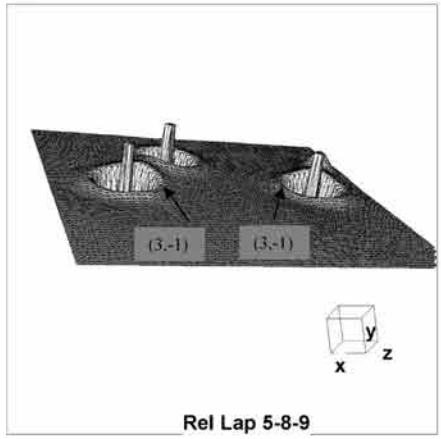

Rel Lap 5-8-9

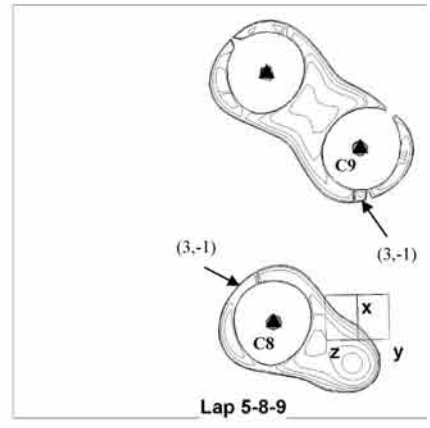

Lap 5-8-9

(c) TS2

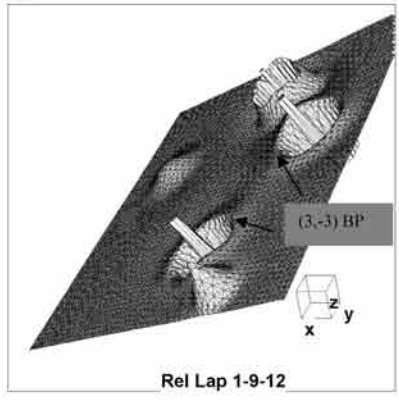

Rel Lap 1-9-12

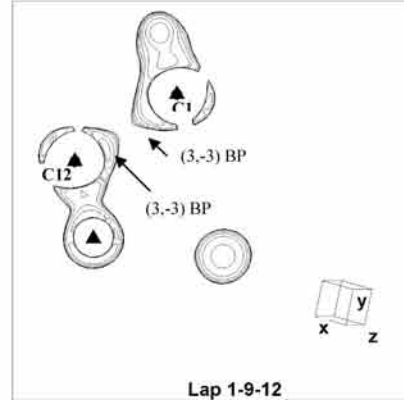

Lap 1-9-12

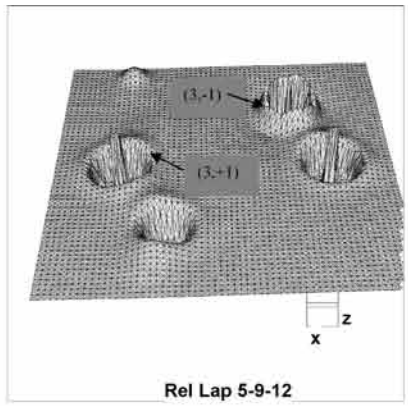

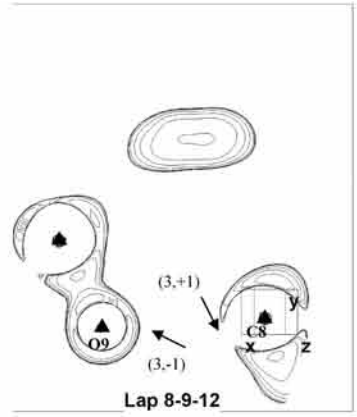

(d) TS4

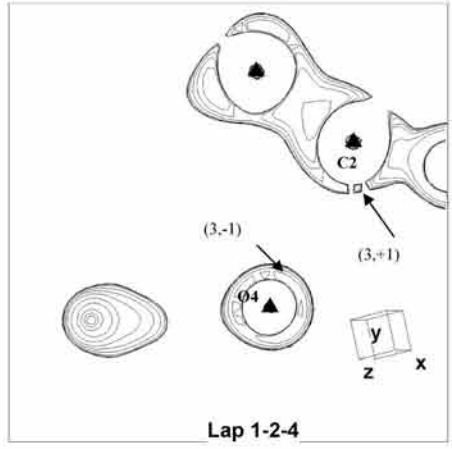

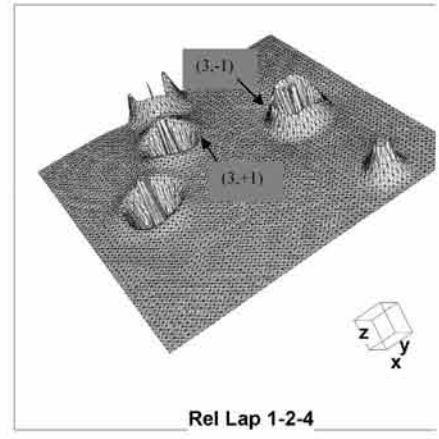

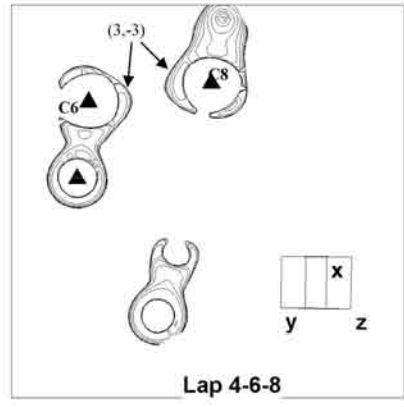

(e) TS5

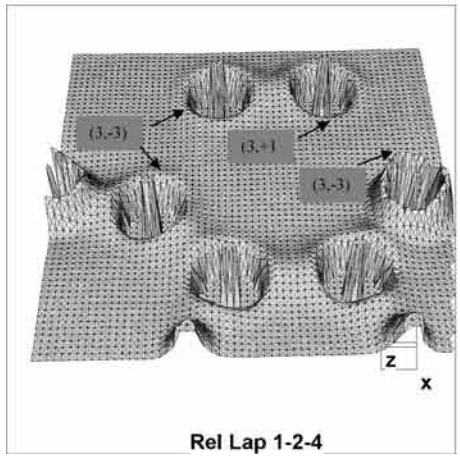

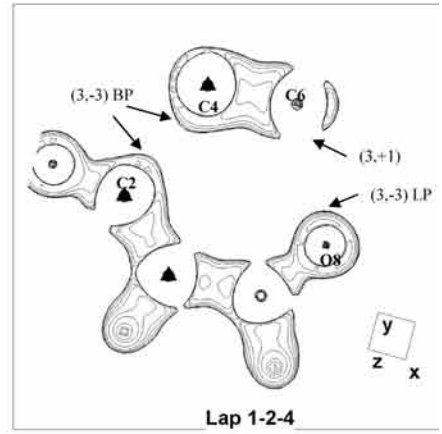

Figure 3. Relief maps and contour plots of the $-\nabla^2\rho(\mathbf{r})$ evaluated in the planes for atoms involved in the bond formation in selected TS structures computed at B3LYP/6-311++G(d,p).

(a) **Reaction 1**

1. Reac1 →TS1 (p.60) E=-234.644826 au

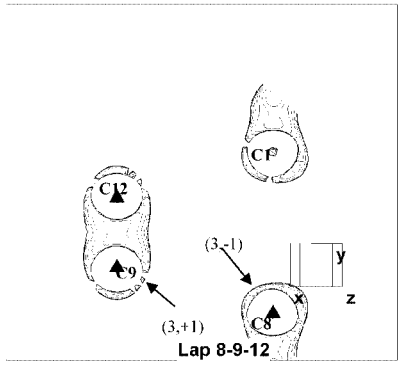

2. Reac1 →TS1 (p.20) E=-234.628293 au

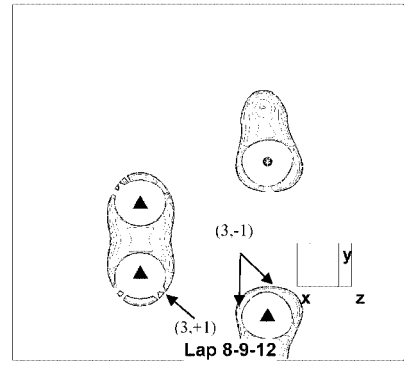

3. Reac1 →TS1 (p.10) E=-234.621022 au

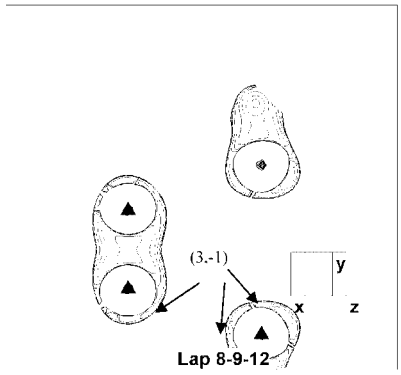

4.TS1 →prod (p.10) E=-234.623718 au

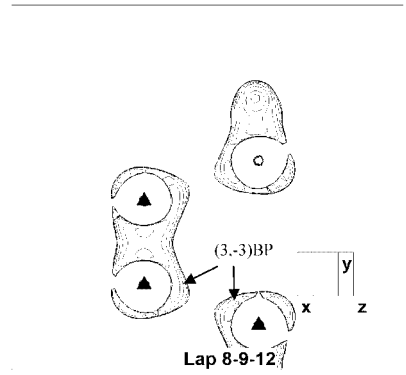

5. TS1 (p.15) →prod E=-234.633025 au

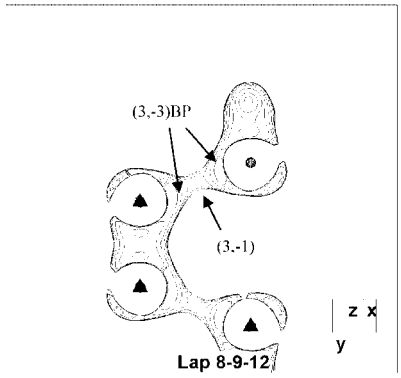

6. TS1 (p.20) →prod E=-234.645033 au

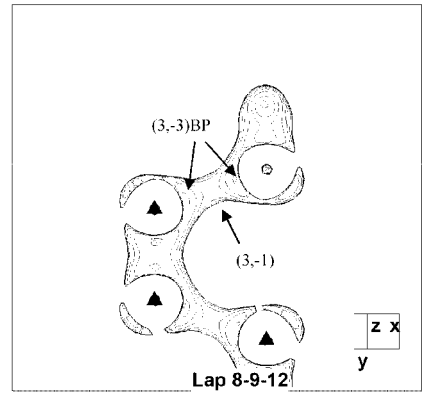

(b) **Reaction 6**

1. Reactant E=-380.5576821au

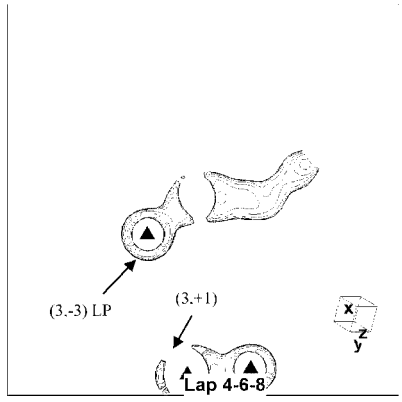

2. Reactant E=-380.5576821au

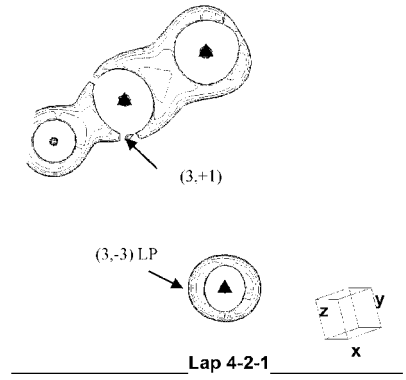

3. Reac6→TS6 (p.40) E=-380.548674 au

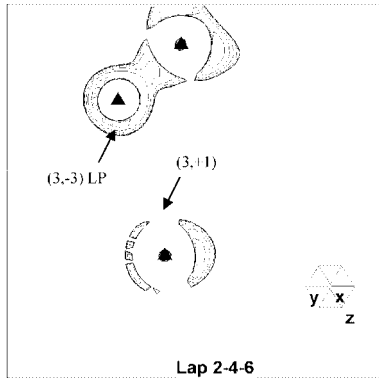

4. Reac6 →TS6 (p.40) E=-380.548674 au

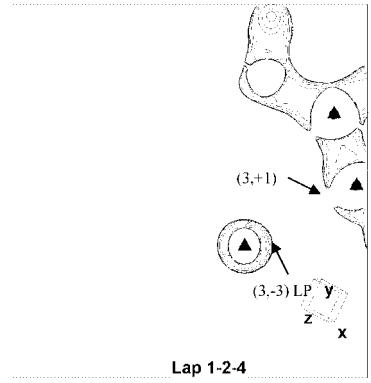

5. TS6→ prod (p.15) E=-380.550546 au

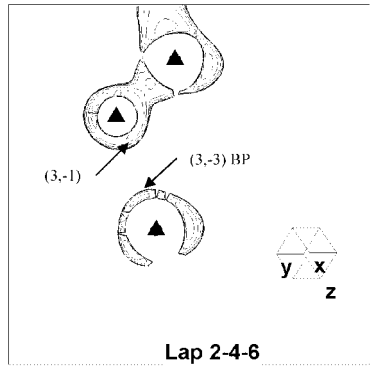

6. TS6→ prod (p.20) E=-380.553913 au

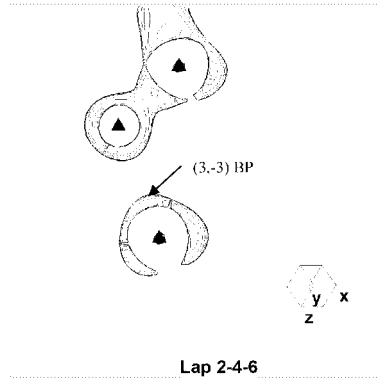

7. TS6→ prod (p.35) E= -380.572722

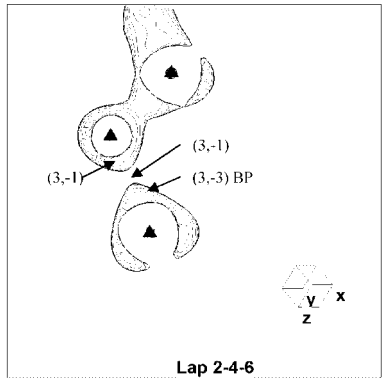

(c) **Reaction 2**

1. Reac →TS2 (p.20) E=-270.55683 au

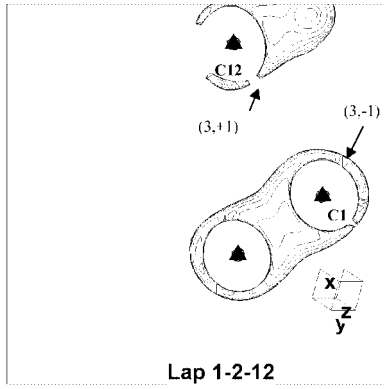

2. Reac→TS2 (p.20) E=-270.55683 au

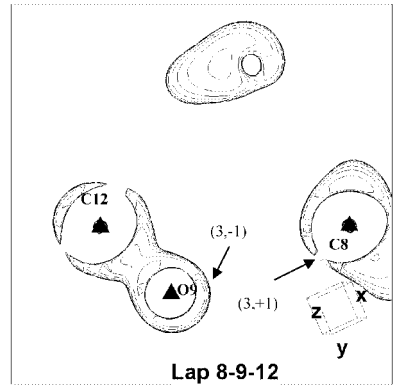

3. Reac →TS2 (p.10) E=-270.548874 au

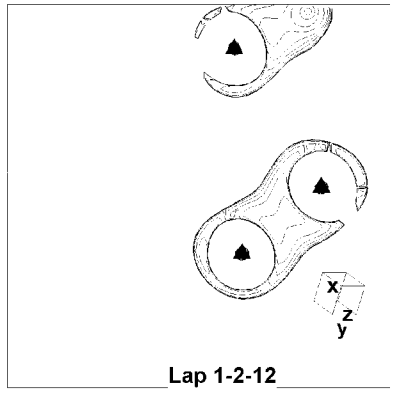

4. Reac → TS2 (p.10) E=-270.548874 au

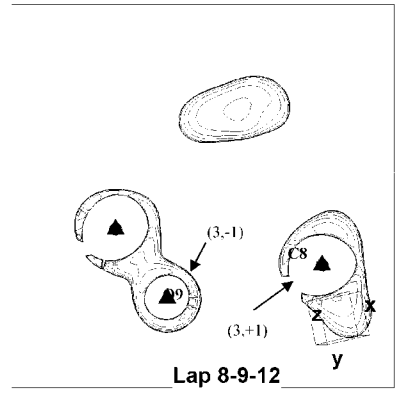

5. TS2→ Prod (p.38) E==-270.548906 au

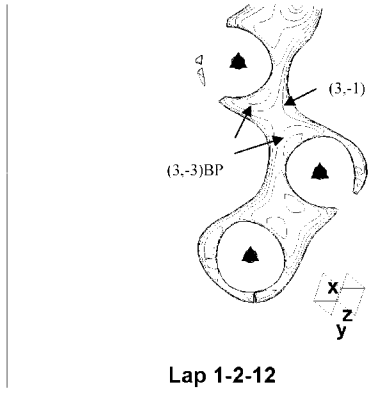

6. TS2→ Prod (p.38) E==-270.548906 au

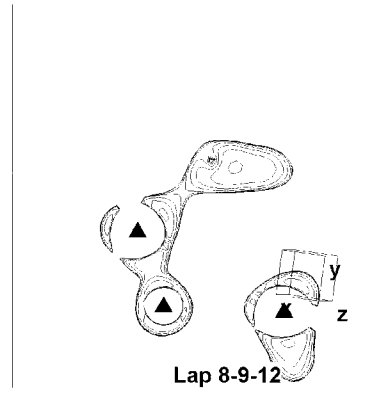

(d) **Reaction 4**

1. Reactant E=-344.6116571 au

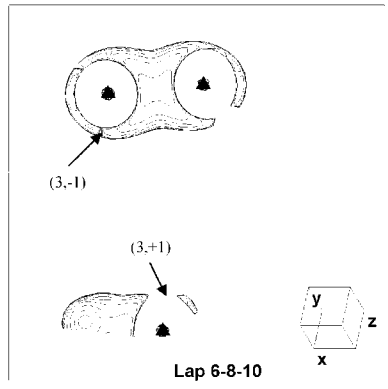

2. Reactant E=-344.6116571 au

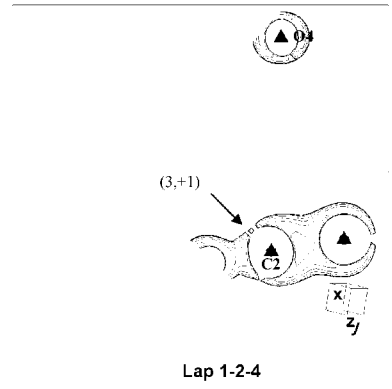

3. Reac4→ TS4 (p.20) E=- 344.598196 au

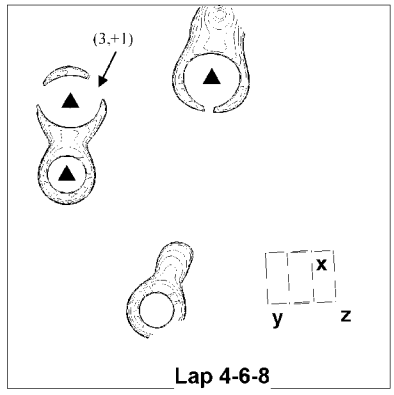

4. Reac4→ TS4 (p.20) E=- 344.598196 au

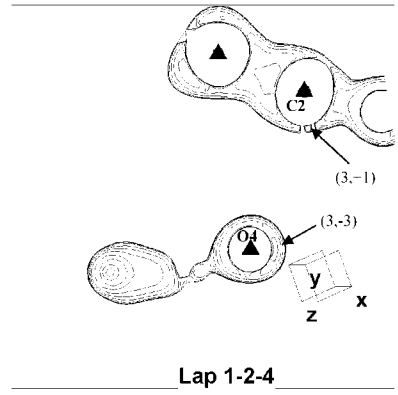

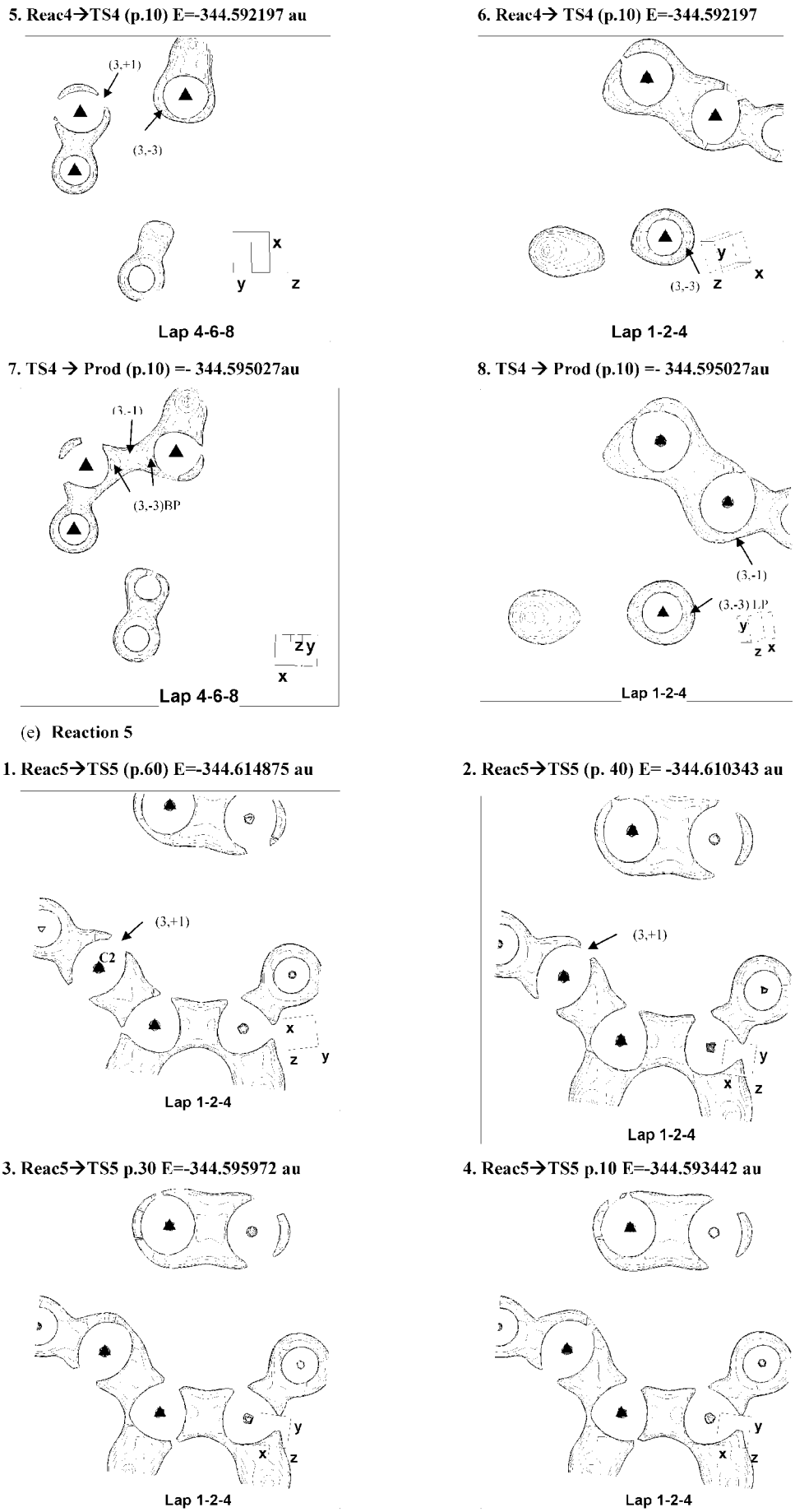

Figure 4. Contour plots of the $L(\boldsymbol{r}) = -\nabla^2\rho(\boldsymbol{r})$ evaluated in planes of the forming bonds for different points along the IRC for reactions 1, 2, 4, 5, and 6 of Scheme 1 at MP2/6-311++G(d,p)//B3LYP/6-311++G(d,p) level (the energy shown is the DFT value).

same CPs and gradient paths[39] (see Figure 2). On the other hand, the IRC for **TS1**, **TS2**, **TS3**, **TS5**, and **TS7** evolved to minima that upon optimization were stabilized by some kind of H interactions between the fragments. These H interactions are not usual because they are between carbon atoms and have been encountered in in-bicyclo[4,4,4]-1-tetradecyl cation.[55] Nevertheless, they fall into the class of intermolecular interactions that are found in van der Waals complexes[41] (for instance, for vdW-**TS1** H15−C2 BCP, $\rho(\boldsymbol{r}) = 0.00521$ au and $\nabla^2\rho(\boldsymbol{r}) = 0.01561$ au and for H14−C5 BCP, $\rho(\boldsymbol{r}) = 0.00437$ au and $\nabla^2\rho(\boldsymbol{r}) = 0.01164$ au at MP2/6-311++G(d,p)). In view of these results, it would seem that in true pseudopericyclic processes (**TS6**, **TS8**), the molecular structure persists from reactants to the TSs uphill, being thus homeomorphic along the reaction coordinate. However, in pericyclic processes (represented by **TS1**, **TS2**, and **TS3**), the evolution is diverse (see below the analysis of $L(\boldsymbol{r})$). In other cases, such as **TS5**, the geometry is entirely lost in the reactant, and **TS4** exhibits a similar but not an homeomorphic molecular structure because not all the CPs of $\rho(\boldsymbol{r})$ are located.

Topology of $\nabla^2\rho(\boldsymbol{r})$. In Figure 1, the CPs of $L(\boldsymbol{r})$ considered to be involved in each process are plotted together with the geometry of the corresponding TS. Relief maps and contour plots of $L(\boldsymbol{r})$ for selected TSs (i.e., **TS6** as pseudopericyclic representative, **TS1** and **TS2** as pericyclic representatives, and **TS4** and **TS5** as representatives of intermediate cases) evaluated in the planes containing the bonds being formed in the reaction coordinates are shown in Figure 3 (the rest are collected in Figure S3 in the Supporting Information). In Figure 4, several contour plots along the reaction coordinate obtained from the IRC calculations for **TS1**, **TS6**, **TS2**, **TS4**, and **TS5** are depicted. As we will see, diverse reaction mechanisms can be observed for pericyclic and pseudopericyclic processes.

As it was indicated above, the laplacian $\nabla^2\rho(\boldsymbol{r})$ determines where the charge density is locally condensated and depleted. Interestingly, diverse patterns of charge condensation appear for pseudopericyclic processes, such as **TS6** and **TS8.** In these cases, the alignment of a hole (a (3, +1) CP) with a lump (a (3, −3) LP) is detected in the topology of $-\nabla^2\rho(\boldsymbol{r})$ with a (3, −1) CP in between as opposed to the metal D−A complexes,[40] and they will be referred to as pseudopericyclic contacts. On the other hand, the pericyclic **TS1** and **TS3** display two (3, −1) CPs for each forming bond that can become true bonding (3, −3) for other TSs (as in **TS5** or **TS7**). This type of contact will be referred to as pericyclic contact. Apart from the pure pseudopericyclic (**TS6** and **TS8**) and pericyclic (in principle only **TS1** and **TS3**), the other cases display both types of contacts, although some subtle differences are found. Let us discuss these findings in more details.

As can be clearly seen in Figure 3, for pseudoperyciclic TSs (such as **TS6** and **TS8**), a nonbonded CC, a (3, −3) LP, or a lump (for the heteroatom) in $L(\boldsymbol{r})$ is facing a depletion of charge or a hole in the VSCC of C atom for both contacts (see planes 8−6−4, 4−2−1, and 4−6−2 for **TS6** Figure 3a and **TS8** in Figure S3 in the Supporting Information) but in reverse fashion (see also Figure 1). In the 4−2 contact, the ketene carbon acts as an acid, whereas in the 6−8 contact, the formyl carbon acts as such instead. Therefore, the donation of charge is balanced between both fragments through two pseudopericylic contacts that act in opposite directions.

The behaviour of $L(\boldsymbol{r})$ along the reaction coordinate follows the same pattern as that of the charge density, $\rho(\boldsymbol{r})$: there is practically no change in the topology of $L(\boldsymbol{r})$ from the reactant to the TS uphill. In the reactant, both pseudopericyclic contacts are already present as can be clearly appreciated in Figure 4b.1 and 4b.2. One of the contacts exhibits a better alignment of the lump and hole than the other ($\angle 4-6-8-10 = 13°$ and $\angle 6-4-2-1 = -87°$). It is worth noting that the bond formation starts once the transition region is surpassed (see contour plots in Figure 4b.5 for p.15) until the (3, –3) BP appear together with the (3, −1) CP associated to the BCP of $\rho(\boldsymbol{r})$ (p.20 in Figure 4b.6). In the last point reported here (p.35 in Figure 4b.7, 2.7 kcal above the product), the typical pattern of (3, −3)−(3, −1)−(3, −1) points for the ether-type bonds is located.

On the other hand, **TS1** is the TS of a prototypical pericyclic process. The topology of $-\nabla^2\rho(\boldsymbol{r})$ for this TS (see Figure 1) does not present any (3, −3) BPs in the VSCC of each atom (namely, C8−C9 and C12−C1) but two (3, −1) CPs for each terminal carbon atom (see Figure 1) forming an angle of about 60°. These points are saddle points and indicate that the C atoms are suffering pyramidalization, and in between, must appear a (3, −3) BP to eventually form a tetrahedral carbon atom (see Scheme 2). Moreover, in the middle of the interaction line, there is a triplet of points (3, −1)−(3, −3)−(3, −1).

The way uphill from the reactants to the TS departs, as was commented above, from a van der Waals complex stabilized by unusual H interactions. The first point (p.60 in Figure 4a.1) considered in IRC above the minimum is 3.9 kcal/mol, and there is an alignment of a (3, +1)CP with a (3, −1) CP of $L(\boldsymbol{r})$. On going uphill charge density coming from adjacent double bonds fills the hole (see p.20 and p.10 in Figure 4a). In this way starts of the pyramidalization of each terminal atom, which is topologically mirrored in the appearance of the saddle (3, −1) CPs in the VSCC of each carbon atom.

When the transition region is surpassed towards the product of the reaction, the growing accumulation of charge density yields two (3, −3) BPs between the (3, −1) CPs for each pair of bonding atoms (i. e., C8, C9 and C12, C1; compare p.10, p.15, and p.20 of **TS1** → Prod in Figure 4a), and interestingly, the triplet is about to merge in a single point. Moreover, for p.15 and p.20, the correct atomic graph for tetrahedral carbon occurs; that is, three saddle (3, −1) CPs are surrounding each bonding (3, −3) CP (see Scheme 2). The two (3, −3) BPs and the intermediate (3, −1) approach each other as long as the bond is being formed (compare the amount of $\rho(\boldsymbol{r})$ from p.10 to p.20).

By adding a keto group to C1 in the **TS1**, we obtain **TS3** (see Figure 1d). As a matter of fact, this functional group addition seems to destabilized the molecule because the energy barrier predicted at B3LYP/6-311++G(d,p) is 1 kcal/mol greater for the **TS3** (see Table 1). Slight variations in respect to its parent **TS1** in the topology of $L(\boldsymbol{r})$ are detected (compare both structures in Figure 1). First appears a new (3, −3) BP at C4 that is surrounded by three (3, −1) saddle points, indicating the pyramidalization of the carbon atom (see Scheme 2). This change is clearly appreciated from the $\nabla^2\rho(\boldsymbol{r})$ plot in the 1−2−4 plane (Figure S3 in the Supporting Information) and from how the electronic charge accumulation at C2, measured by a (3, −1)CP, comes from the adjacent double bond.

In **TS2**, only one of the lump−hole contacts exists (see plots C5−C9−C12 and C8−O9−C12 in Figure 3c), but as can be distinguished in the contour map of $L(\boldsymbol{r})$ for the plane C8−O9−C12, the VSCC of O9 atom has a torus of charge around the nucleus. Hence, in this case, the lump is not a true maximum but a (3, −1) saddle point. Bader and co-workers denoted these as secondary CCs.[33,40] Moreover, it seems that the hole is not well oriented at the lump. On the other hand, a different contact for C12 and C1 atoms appears (see Figure 3). In this case, a bonding (3, −3) CP of $L(\boldsymbol{r})$ is provided by the

VSCC of each atom. The magnitude of $\nabla^2\rho(\boldsymbol{r})$ for these points are dramatically lower as compared to those of the nonbonding maxima (compare, for instance, the relief maps computed in the C1−C9−C12 plane for **TS2** with that computed in C8−O6−C4 for **TS6**). The analysis of $\rho(\boldsymbol{r})$ rendered a molecular structure for the reactant (see Figure 2) that was stabilized by H interactions (as **TS1** and **TS3**). From Figure 4c, it is seen that the process toward the TS consists in creating the hole at C8 (compare the (3, +1) CP in Figures 4c.2 and 3c) and conversely filling the hole at C12 (compare C12 in Figures 4c.2 and 3c) to eventually be bonded to C1 (compare Figures 4c.1, 4c.3 and 4c.5).

TS4 looks, in principle, topologically equivalent to **TS2** (compare both structures in Figure 1) but eventually will present novel features. First, as has just been commented, the reactant exhibits a geometry similar to that of the TS, hence the low energy barrier found. The topology of $L(\boldsymbol{r})$ renders both type of contacts: a pericyclic one between C6 and C8 and a lump−hole link between C2 and O4 (see contour maps in Figure 3d). The (3, −3) BPs found are surrounded by three saddle (3, −1); therefore, the pyramidalization for both termini is already completed (see Scheme 2). On the other hand, the lump (as in **TS2**) is also a secondary CC, that is, a (3, −1) CP in the VSCC directed at the hole (note in Figure 3 how the (3, −3) LP is perpendicular to the interaction line). It is worth noting that the hole is not wide because it has a certain charge accumulation (hence the (3, −1) CP shown in Figure 1). However, this contact comes from the reactant (see Figure 4d.2) and is very similar to the C2–O4 contact in the reactant of **TS6** (see Figure 4b.2). Remarkably, the link between C6 and C8 in the reactant is also a lump−hole contact and evolves by accumulating charge density so as to form two (3, −3) BPs in the TS as can be seen in Figure 3d. The other contact (between C2 and C4) persists before passing the TS zone in the same fashion as in **TS6** and **TS8**, and the formation of the bond occurs afterward (see Figures 4d.4 and 4d.8.)

TS5 resembles **TS2** in that both types of contacts are also found here (see Figure 1). In one hand, a pseudopericyclic contact is detected between C6 and C8 (see Figure 3e), and on the other hand, the appearance of two bonded (3, −3) CPs configures a pericyclic link. The atomic graphs of C4 and C2 practically correspond to a tetrahedral and trigonal configuration, respectively (see Scheme 2). Interestingly, around the allene carbon of the ketene, unusual special electronic reorganization is found out: the bonded (3, −3) CP that appears here is in turn a hole in **TS6** or **TS8**. Therefore, a rearrangement at the VSCC of this carbon must occur to turn it from acceptor to donor of charge density. This is in fact observed along the reaction coordinate: what at the beginning of the process is a hole will be filled with charge density to be transformed into a (3, −3) BP in the TS (compare the hole at C2 for p.60, p.40, p.30, and p.10 in Figure 4e). As a matter of fact, this could be the reason for the unexpectedly great energy barrier observed for this TS.

TS7 is topologically equivalent to **TS5** except for the pericyclic contact between a (3, −1)CP and a (3, −3) BP (see Figure 1 and planes in Figure S3 in the Supporting Information), indicating that the BP provided by the C2 is not yet formed.

Summary

In this paper, we have carried out a theoretical study of a series of cycloaddition reactions by using the topology of $\rho(\boldsymbol{r})$ and $\nabla^2\rho(\boldsymbol{r})$ in the framework of the QTAIM developed by Bader. At our best level of theory (namely, B3LYP/6-311++G(d,p) and MP2/6-311++G(d,p)), the lowest energy barriers have been found for **TS6** and **TS8**. Some planar TSs (**TS5**) are predicted to lie on the PES over the pericyclic ones. **TS4** has an intermediate value. The analysis of the topology of $\rho(\boldsymbol{r})$ renders interesting points: (1) True pseudopericyclic TSs, such as **TS6** and **TS8**, show a homeomorphism for pseudopericyclic with their respective reactants, and (2) pericyclic processes exhibit H interactions that stabilize the reactant. Nevertheless, the topology of $\rho(\boldsymbol{r})$ does not suffice to explain the differences in behavior, and to get insight into the mechanisms of the reactions, one has to go to the topology of $L(\boldsymbol{r}) = -\nabla^2\rho(\boldsymbol{r})$. In fact, two main different patterns of contacts as reflected in the CPs of $L(\boldsymbol{r})$ of the TSs are found. First, the pericyclic reactions exhibit contacts (referred to as pericyclic contact) where amounts of charge density (reflected in (3, −1) or (3, −3) CPs) appear in both terminal atoms as in **TS1** and **TS3.** On the contrary, a pseudopericyclic contact consists of aligning a hole with a lump as occurs in donor−acceptor complexes, notwithstanding the differences noted above. In terms of CPs, this involves the alignment of a nonbonding (3, −3) CP in the VSCC of the donor (base) with a (3, +1) CP of the acceptor (acid) as in **TS6** and **TS8**. Alternatively, the alignment can also be done between a secondary charge accumulation with the hole, that is, a (3, −1) CP with a (3, +1) as in **TS2** or **TS4**. In intermediate cases, both types of contacts are encountered (such as in **TS2**, **TS4**, **TS5,** and **TS7**). In order to shed further light on mechanistic differences in the processes, the topology of $L(\boldsymbol{r})$ along the IRC was carried out. Interestingly, the pseudopericyclic processes (i.e., **TS6** and **TS8**) are already being linked by the same contacts in the reactant as that in the TS, keeping therefore the molecular structure along the reaction coordinate. Therefore, electronic reorganization hardly occurs, and the energy barriers turn out to be extremely low. On the contrary, true pericyclic reactions usually depart from reactants that are stabilized by different kinds of H interactions and necessitate electronic reorganization throughout the backbones to create the (3, −3) BPs and thus pyramidalize the terminal atoms. Another difference is that for a pseudopericyclic process, the reaction usually takes place once the TS region is surpassed.

When both contacts are of the same kind, one could be sure of dealing with either (true) pericyclic or (true) pseudopericyclic reactions. Among the extreme poles, when both contacts are present, there is a range of possibilities: from TSs with more pericylic flavor or pericyclic character (as **TS1**) to those with more pseudopericyclic flavor (as **TS4**). Nevertheless, in view of our results, the criteria of planarity and of low energy barrier seem to be necessary but not sufficient conditions.

Acknowledgment. S.C.L. thanks SCAI (Málaga) for generously allocated time at Picasso Supercomputer.

Supporting Information Available: This material is available free of charge via the Internet at http://pubs.acs.org.

References and Notes

(1) Lemal, D. *J. Am. Chem. Soc.* **1976**, *98*, 4325.
(2) Birney, D. M.; Wagenseller, P. E. *J. Am. Chem. Soc.* **1994**, *116*, 6262.
(3) Birney, D. M.; Ham, S.; Unruh, G. R. *J. Am. Chem. Soc.* **1997**, *119*, 4509.
(4) Birney, D. M.; Xu, X.; Ham, S. *Angew. Chem., Int. Ed.* **1999**, *38*, 189.
(5) Birney, D. M. *J. Am. Chem. Soc.* **2000**, *122*, 10917.
(6) Shumway, W. W.; Dalley, N. K.; Birney, D. M. *J. Org. Chem.* **2001**, *66*, 5832.
(7) Zhou, C.; Birney, D. M. *J. Am. Chem. Soc.* **2002**, *124*, 5237.

(8) Unruh, G. R.; Birney, D. M. *J. Am. Chem. Soc.* **2003**, *125*, 8529.
(9) Wei, H.; Zhou, C.; Ham, S.; White, J. M.; Birney, D. M. *Org. Lett.* **2004**, *23*, 4289.
(10) Sadasivam, S. V.; Birney, D. M. *Org. Lett.* **2005**, *26*, 5817.
(11) Cabaleiro-Lago, E. M.; Rodríguez-Otero, J.; González-López, I.; Peña-Gallego, A.; Hermida-Ramón, J. *J. Phys. Chem. A* **2005**, *109*, 5636.
(12) Rodríguez-Otero, J.; Cabaleiro-Lago, E. M. *Angew. Chem., Int. Ed.* **2002**, *41*, 1147.
(13) Rodríguez-Otero, J.; Cabaleiro-Lago, E. M. *Chem. Eur. J.* **2003**, *9*, 1837.
(14) Cabaleiro-Lago, E. M.; Rodríguez-Otero, J.; Hermida-Ramón, J. M. *J. Phys. Chem. A* **2003**, *107*, 4962.
(15) Rodríguez-Otero, J.; Cabaleiro-Lago, E. M.; Hermida-Ramón, J. M.; Peña-Gallego, A. *J. Org. Chem.* **2003**, *68*, 8823.
(16) Montero-Campillo, M. M.; Rodríguez-Otero, J.; Cabaleiro-Lago, E. M. *J. Phys. Chem. A* **2004**, *108*, 8373.
(17) Cabaleiro-Lago, E. M.; Rodríguez-Otero, J.; Varela-Varela, S. M.; Peña-Gallego, A.; Hermida-Ramón, J. *J. Org. Chem.* **2005**, *70*, 392.
(18) Herges, R.; Geuenich, D. *J. Phys. Chem. A* **2001**, *105*, 3214.
(19) Kimball, D. B.; Weakley, T. J. R.; Herges, R.; Haley, M. M. *J. Am. Chem. Soc.* **2002**, *124*, 13463.
(20) Geuenich, D.; Hess, K.; Köhler, F.; Herges, R. *Chem. Rev.* **2005**, *105*, 3758.
(21) López, C. S.; Faza, O. N.; Cossío, F. P.; Cork, D. M.; de Lera, A. R. *Chem. Eur. J.* **2005**, *11*, 1734.
(22) Rode, J. E.; Dobrowolski, J. Cz. *J. Phys. Chem. A* **2006**, *110*, 207.
(23) Rode, J. E.; Dobrowolski, J. Cz. *J. Phys. Chem. A* **2006**, *110*, 3723.
(24) Chamorro, E.; Santos, J. C.; Gómez, B.; Contreras, R.; Fuentealba, P. *J. Phys. Chem. A* **2002**, *106*, 11533.
(25) Chamorro, E. *J. Chem. Phys.* **2003**, *118*, 8687.
(26) Chamorro, E.; Notario, R. *J. Phys. Chem. A* **2004**, *108*, 4099.
(27) Chamorro, E.; Notario, R. *J. Phys. Chem. A* **2005**, *109*, 7594.
(28) Cárdenas, C.; Chamorro, E.; Notario, R. *J. Phys. Chem. A* **2005**, *109*, 4352.
(29) Matito, E.; Poater, J.; Durán, M.; Solá, M. *ChemPhysChem* **2006**, *7*, 111.
(30) Savin, A.; Nesper, R.; Wengert, S.; Fässler, T. F. *Angew. Chem., Int. Ed. Engl.* **1997**, *36*, 1808.
(31) Alajarín, M.; Ortín, M. M.; Sánchez-Andrada, P.; Vidal, A.; Bautista, D. *Org. Lett.* **2005**, *7*, 5281.
(32) Bader, R. F. W. *Atoms in Molecules: A Quantum Theory*. Oxford University Press: Oxford, UK 1990. A recent survey of QTAIM theory is due to Popelier P. L. A., Aicken F. M., and O'Brien S. E. Published in *Chemical Modelling: Applications and Theory*; Vol. 1. See also the introductory book by Popelier, P. *Atoms in Molecules. An introduction*; Prentice Hall: New York, **2000** and the paper by Merino G., Vela A., Heine T., *Chem. Rev.* **2006**, *105*.
(33) Bader, R. F. W.; Chang, C. *J. Phys. Chem.* **1989**, *93*, 2946.
(34) Laidig, K. E.; Bader, R. F. W. *J. Am. Chem. Soc.* **1991**, *113*, 6312.
(35) Krug, J. P.; Popelier, P. L. A.; Bader, R. F. W. *J. Phys. Chem.* **1992**, *96*, 7604.
(36) Chang, C.; Bader, R. F. W. *J. Phys. Chem.* **1992**, *96*, 1654.
(37) Wang, C.-C.; Wang, Y.; Liu, H-J.; Lin, K.-J.; Chou, L.-K.; Chan, K. S. *J. Phys. Chem. A* **1997**, *101*, 8887.
(38) Popelier, P. L. A. *Coord. Chem. Rev.* **2000**, *197*, 169.
(39) Malcolm, N. O. J.; Popelier, P. L. A. *J. Phys. Chem. A* **2001**, *105*, 7638.
(40) See Cortés-Guzmán, F.; Bader, R. F. W. *Coord. Chem. Rev.* **2005**, *249*, 633 and references therein.
(41) Bone, R. G.; Bader, R. F. W. *J. Phys. Chem.* **1996**, *100*, 10892.
(42) Bader, R. F. W. *J. Phys. Chem. A* **1998**, *102*, 7314.
(43) Bader, R. F. W.; Fang, D.-C. *J. Chem. Theory Comput.* **2005**, *1*, 403.
(44) Cremer, D.; Kraka, E. *J. Am. Chem. Soc.* **1985**, *107*, 3800.
(45) Gibbs, G. V.; Spackman, M. A.; Jayatilaka, D.; Rosso, K. M.; Cox, D. F. *J. Phys. Chem. A* **2006**, *110*, 12259.
(46) Frisch, M. J.; Trucks, G. W.; Schlegel, H. B.; Scuseria, G. E.; Robb, M. A.; Cheeseman, J. R.; Zakrzewski, V. G.; Montgomery, J. A., Jr.; Stratmann, R. E.; Burant, J. C.; Dapprich, S.; Millam, J. M.; Daniels, A. D.; Kudin, K. N.; Strain, M. C.; Farkas, O.; Tomasi, J.; Barone, V.; Cossi, M.; Cammi, R.; Mennucci, B.; Pomelli, C.; Adamo, C.; Clifford, S.; Ochterski, J.; Petersson, G. A.; Ayala, P. Y.; Cui, Q.; Morokuma, K.; Malick, D. K.; Rabuck, A. D.; Raghavachari, K.; Foresman, J. B.; Cioslowski, J.; Ortiz, J. V.; Stefanov, B. B.; Liu, G.; Liashenko, A.; Piskorz, P.; Komaromi, I.; Gomperts, R.; Martin, R. L.; Fox, D. J.; Keith, T.; Al-Laham, M. A.; Peng, C. Y.; Nanayakkara, A.; Gonzalez, C.; Challacombe, M.; Gill, P. M. W.; Johnson, B. G.; Chen, W.; Wong, M. W.; Andres, J. L.; Head-Gordon, M.; Replogle, E. S.; Pople, J. A. *Gaussian 98*, revision A.11; Gaussian, Inc.: Pittsburgh, PA, 1998.
(47) Frisch, M. J.; Trucks, G. W.; Schlegel, H. B.; Scuseria, G. E.; Robb, M. A.; Cheeseman, J. R.; Montgomery, J. A., Jr.; Vreven, T.; Kudin, K. N.; Burant, J. C.; Millam, J. M.; Iyengar, S. S.; Tomasi, J.; Barone, V.; Mennucci, B.; Cossi, M.; Scalmani, G.; Rega, N.; Petersson, G. A.; Nakatsuji, H.; Hada, M.; Ehara, M.; Toyota, K.; Fukuda, R.; Hasegawa, J.; Ishida, M.; Nakajima, T.; Honda, Y.; Kitao, O.; Nakai, H.; Klene, M.; Li, X.; Knox, J. E.; Hratchian, H. P.; Cross, J. B.; Bakken, V.; Adamo, C.; Jaramillo, J.; Gomperts, R.; Stratmann, R. E.; Yazyev, O.; Austin, A. J.; Cammi, R.; Pomelli, C.; Ochterski, J. W.; Ayala, P. Y.; Morokuma, K.; Voth, G. A.; Salvador, P.; Dannenberg, J. J.; Zakrzewski, V. G.; Dapprich, S.; Daniels, A. D.; Strain, M. C.; Farkas, O.; Malick, D. K.; Rabuck, A. D.; Raghavachari, K.; Foresman, J. B.; Ortiz, J. V.; Cui, Q.; Baboul, A. G.; Clifford, S.; Cioslowski, J.; Stefanov, B. B.; Liu, G.; Liashenko, A.; Piskorz, P.; Komaromi, I.; Martin, R. L.; Fox, D. J.; Keith, T.; Al-Laham, M. A.; Peng, C. Y.; Nanayakkara, A.; Challacombe, M.; Gill, P. M. W.; Johnson, B.; Chen, W.; Wong, M. W.; Gonzalez, C.; Pople, J. A. *Gaussian 03*, revision B.04; Gaussian, Inc.: Wallingford, CT, 2004.
(48) Biegler-König, F. *AIM*, Version 1; Bielefeld University: Germany, 2000.
(49) (a) Popelier, P. L. A.; Bone, R. G. A. MORPHY98. *Comp. Phys. Comm.* 1996, *93*, 212. (b) Popelier, P. L. A. *Theor. Chim. Acta* **1994**, *87*, 465. (c) Popelier, P. L. A. *Mol. Phys.* **1996**, *87*, 1169. (d) Popelier, P. L. A. *Comp. Phys. Comm.* **1998**, *108*, 180. (e) Popelier, P. L. A. *Can. J. Chem.* **1996**, *74*, 829.
(50) (a) Becke, A. D. *J. Chem. Phys.* **1993**, *98*, 5648. (b) Becke, A. D. *Phys. Rev.* **1988**, *38*, 3048. (c) Lee, C.; Yang, W.; Parr, R. G. *Phys. Rev. B* **1988**, *37*, 785.
(51) Hehre, W. J.; Radom, L.; Pople, J. A.; Schleyer, P. v. R. *Ab Initio Molecular Orbital Theory*; John Wiley & Sons Inc.: New York, 1986.
(52) Shaftenaar, G. *MOLDEN*, Version 3.7 for Windows 95; CAOS/CAMM Center: Nijmegen.
(53) Fukui, K. *Acc Chem. Res.*, **1981**, *14*, 363. The IRC calculations are implemented in Gaussian following the González and Schlegel algorithm. (a) González, C.; Schlegel, H. B. *J. Chem. Phys.* **1989**, *90*, 2154. (b) González, C.; Schlegel, H. B. *J. Phys. Chem.* **1990**, *94*, 5523.
(54) Matta, C. F.; Hernández-Trujillo, J.; Tang, T-H.; Bader, R. F. W. *Chem. Eur. J.* **2003**, *9*, 1940.
(55) DuPré, D. B. *J. Phys. Chem. A* **2005**, *109*, 622.

JP711565G